Journal of Molecular Modeling (2019) 25: 302
https://doi.org/10.1007/s00894-019-4185-2

ORIGINAL PAPER

Density functional theory study of π-aromatic interaction of benzene, phenol, catechol, dopamine isolated dimers and adsorbed on graphene surface

Elizane E. de Moraes[1] · Mariana Z. Tonel[1] · Solange B. Fagan[2] · Marcia C. Barbosa[1]

Received: 12 March 2019 / Accepted: 27 August 2019 / Published online: 7 September 2019
© Springer-Verlag GmbH Germany, part of Springer Nature 2019

Abstract

We analyze the influence of different groups on the intermolecular energy of aromatic homodimers and on the interaction between a single aromatic molecule and a graphene surface. The analysis is performed for benzene, phenol, catechol, and dopamine. For calculating the energies, we employ density functional theory within the local density approximation (LDA-DFT). Our results show that the lowest intermolecular energies between the aromatic molecules are related to the T-shaped configurations. This lower energy results from the quadrupole interaction. In the case of the interaction between the graphene sheet and the aromatic molecules, the lowest energy configuration is the face to face. The adsorption energy of a molecule on a graphene surface involves $\pi - \pi$ interactions that explain the face to face arrangement. These results provide insight into the manner by which substituents can be utilized in crystal engineering, supramolecular chemistry, bioinspired materials, formation of various molecular clusters, parameterization of force fields suitable for classical simulations, and design of novel sensing, drug delivery, and filters based on graphene.

Keywords Graphene · Aromatic homodimers · Density functional theory · Parameterization of force fields suitable for classical simulations

Introduction

Carbon is a very versatile and important chemical element, not only because when combined with other elements it becomes the building block of organic compounds but also because of its ability to form a variety of allotropic forms [1–3]. Moreover, depending on the arrangement of the atoms in the different allotropic forms, the resulting molecule presents different physical properties. One of the last allotropes to be obtained experimentally was the graphene (GR) [4].

Graphene has attracted interest from the scientific community due to its electronic and structural characteristic [5, 6]. This crystalline allotrope of carbon has one layer of atoms arranged in a honeycomb lattice in which the electrons are free in two directions and confined in one that gives strength to the structure. This monolayer has a huge and flexible surface area and huge electric and thermal conductivity which enables a variety of applications from sensors to drug delivery [7–9]. The idea is that the interaction between the graphene and other materials can be activated or suppressed by the environment. Therefore, it is relevant to understand the interaction between graphene and other materials, particularly the aromatic molecules [10–17].

Aromatic compounds are candidates for drug delivery due to their presence in a number of biological processes. In order to understand how the graphene might capture and release the molecules, it is relevant to obtain which is the orientation of the molecules close to the graphene surface. In very dilute systems and at very low temperatures,

✉ Elizane E. de Moraes
elizane.fisica@gmail.com

Mariana Z. Tonel
marianaztonel@gmail.com

Solange B. Fagan
solange.fagan@gmail.com

Marcia C. Barbosa
marcia.barbosa@ufrgs.br

[1] Instituto de Física, Universidade Federal do Rio Grande do Sul, Caixa Postal 15051, Porto Alegre, Rio Grande do Sul, 91501-970, Brazil

[2] Universidade Franciscana, Santa Maria, RS 97010-032, Brazil

in which only the interaction between the molecule and the graphene is taken into account, the lowest energy configurations are the aromatic ring parallel or perpendicular to the confining surface [18]. However, other orientations become relevant between molecule-molecule and molecule-graphene systems if temperature is taken into account [19–22].

A good parametrization method to account for the molecule-graphene interaction is still missing. While the atomistic approaches fit the interaction parameters with experimental results at a certain temperature, the first principle calculations focus on the zero temperature configurations what captures the minimum energy configurations. The idea here is to combine both approaches by selecting representative low energy intermolecular geometries to parametrize an atomistic interaction [23–26] which is adequate to capture essential trends of the structural properties in a large range of the temperatures and pressures for a mixture.

In the bulk, the aromatic molecule intermolecular interactions are responsible for the formation of clusters [27–30], the supramolecular assembly phenomena, [31] the formation of structures [32], the crystal packaging [33], and the engineering of nanomaterials [34]. These structures result from the competition between the interactions H–π [35, 36], π–π stacking, and H–H [37–41]. Thus, investigating the bulk system in classical simulations, so that the classic force fields provide information on the most probable configurations at zero temperature, gives an understanding of the origin of the molecular structure computed by the radial distribution function for aromatic molecules which depend on the competitions between the interactions in each configuration of the system.

In this paper, we address two questions which are relevant for the interaction of molecules and the graphene. We compare the molecule-molecule and molecule-graphene energies when the orientations and distance are changed. The idea is to identify the lowest energy molecule-molecule and molecule-graphene configurations. The other question is the impact of the competition between the $\pi - \pi$ and the H-π interactions in the definition of the optimal molecule-molecule and molecule-graphene configurations. In order to answer these two issues, we evaluate the interaction between two molecules of benzene (BZ), phenol, catechol or dopamine (DA) in different configurations. Then we compare this intermolecular energy with the energy of the same molecule when interacting with a GR sheet. We focus on the influence of the interactions X–π (X = CH, OH, NH_2), $\pi - \pi$, and X–X in the molecule-molecule and molecule-graphene interactions to identify the more relevant configurations in both cases. This allows us to understand the effect of these groups in the adsorption of these molecules in graphene. The remaining of the paper goes as follows. In the "Model and methods" section, the models and methods are presented; in the "Results and discussion" section, the results are discussed; and in the "Conclusions" section, we present our conclusions.

Model and methods

We studied the influence of the interactions X–X, X–π (X = CH, OH, two OH, NH_2), and $\pi - \pi$ on the aromatic ring in the interaction of molecule–molecule (homodimers) and molecule–graphene versus distance through density functional theory (DFT) [42, 43], implemented in the SIESTA (Spanish Initiative for the Electronic Simulations of Thousands of Atoms) code [44]. The electronic, energetic, and structural properties were analyzed solving the self-consistent Kohn–Sham equations. In all calculations, a double ζ plus a polarized function (DZP) was used for the numerical basis set. In order to describe the exchange and correlation potential (V_{xc}), we investigated the performance of the three functional implemented in the SIESTA: (i) the LDA with the Perdew and Zunger (PZ) parametrization [45] the correction to basis set superposition error (BSSE corrected) [46], (ii) the generalized gradient approximation (GGA) with the Perdew, Burke, and Ernzerhof (PBE) version [47], and (iii) GGA dispersion correction [48] with the Perdew, Burke, and Ernzerhof (PBE) version.

In this work, we adopted the LDA functional with the correction to basis for two complementary reasons. First, when compared with the other two options above, it gives a better agreement with the literature [23, 24, 49, 50] for the minimum energies configuration. The second reason is that since we want to compare the energies between the molecule–molecule and the molecule–graphene cases, the energy has to go to zero at very large distances. This constraint is important because our proposal is to construct a force field from first principles.

In order to represent the electronic charge in real space, a grid cutoff of 200 Ry was used. All of the studied systems present a neutral charge in the initial electronic configuration. The isolated molecules and graphene structures were relaxed until the residual forces were less than 0.05 eV $Å^{-1}$ in all atomic coordinates. Additionally, graphene studied shows 144 carbon atoms to carry out the simulations of molecule–graphene we used periodic boundary conditions, the cell had dimensions of $25.94 \times 40.00 \times 14.98$ $Å^3$, also called supercell method. In the case of the molecule–molecule interaction, we use a super cell of $40 \times 40 \times 40$ $Å^3$). The isolated molecules are relaxed residual lower forces than 0.05 eV/Å and then kept frozen upon adsorption on the graphene, and in the interactions of the homodimers. The distance (r) between the homodimers and the molecule–graphene refers

to the minimum atom–atom distance of each configuration studied.

The relative numerical accuracy on the interaction energy versus distance, computed with the correction to the basis set superposition error (BSSE corrected) is estimated to be of the order of around 0.96 kJ/mol.

For the interaction energy calculations, we used the following equation through BSSE (basis set superposition error) corrected for all calculations with the counterpoise method [46]:

$$E = E(A + B) - E(A + B_{\text{ghost}}) - E(B + A_{\text{ghost}}). \quad (1)$$

This correction is performed starting from the initial geometry of the AB system and calculating the total energy of system A, considering the whole set of base functions, where the set of base functions B is in the position corresponding to system B, without the explicit presence of the atoms. The same occurs in the calculation of system B. The system with negative binding energies implies attractive interaction.

Results and discussion

First, we selected representative parallel and T-shaped intermolecular configurations for benzene (BZ), phenol, catechol, or dopamine (DA). Thereafter, we calculated the potential-energy curves of these configurations as a function of the distance r between the molecule–molecule and molecule–graphene via DFT formalism with the correction to basis as indicated in the Eq. 1.

Intermolecular interactions

For the benzene–benzene interaction, we considered five basic configurations: (a) face to face (BZ-BZ_FF), (b) slipped parallel (BZ-BZ_SP), (c) side by side (BZ-BZ_SS), (d) T-shaped (BZ-BZ_TS$_1$), and (e) T-shaped displaced (BZ-BZ_TSD). The interaction energy curves calculated between the benzene dimers are illustrated in Fig. 1, in units kJ/mol.

The side by side configuration showed in Fig. 1c is the least attractive since its energy major configuration is the H–H repulsion. The T-shaped and the T-shaped displaced configurations illustrated in Fig. 1d and e exhibit the lowest energies when compared with other configurations. The attractive behavior at very low distances in this case can be explained in terms of the favorable electrostatic interaction between the negatively charged π-cloud located in the center of the lower ring and the positively charged hydrogen atom of the other subsequent. The most stable configuration is the BZ-BZ_TS$_1$ which optimizes the distance between the H–π interactions. The total energy for the BZ-BZ_TS$_1$ is $-$ 9.0 kJ/mol at r = 2.5 Å, while for BZ-BZ_TSD configuration the energy is about $-$ 7.2 kJ/mol at r = 2.5 Å.

The face to face configurations BZ-BZ_FF and BZ-BZ_SP (Fig. 1a and b) show the minimum energies at $-$ 2.92 kJ/mol at (r = 3.75 Å) and $-$ 6.63 kJ/mol at (r = 3.5 Å), respectively. These energies result to the attractive π–π stacking. The difference between the two parallel configurations occurs because the displacement decreases the quadrupolar repulsion between benzene dimer and adds an electrostatic attraction between the positive H and the negative π-cloud [51, 52].

In order to confirm that the configurations with lowest energies are the TS, TSD, and the SP, we compared our results with the energies obtained using other functionals. Cacelli et al. [23, 49] found that the interacting energy of the BZ-BZ_SP, BZ-BZ_TS$_1$, and BZ-BZ_FF configurations for benzene were around $-$ 7.0, $-$ 9.8, and $-$ 4.0 kJ/mol, respectively. These values were computed by the MP2/6-31G (BZ-BZ_TS$_1$) and MP2/CAM-B3LYP-D3 (BZ-BZ_FF and BZ-BZ_SP) theory. The same behavior is observed in other theoretical approaches [52–54]. Comparison with the results of Cacelli et al. [23, 49] shows energy differences that are less than 0.8 [49], 1.08 [23], 1.37 [23] kJ/mol, respectively. Grover et al. [25] reported that the experimental binding energy TS of the benzene dimer was $-$ 10.05 $\pm$ 1.67 kJ/mol. Tsuzuki et al. [55] reported that the minimum value for the interacting energy of the BZ-BZ_FF is around $-$ 6.19 ($-$ 3.59) kJ/mol computed by CCSD(T)/6-31G (MP2/6-31G*) theory gives similar behavior as our results. In general, chemical bonding and electron transfer can be described well within the LDA functional.

When compared with more sophisticated theories, for instance, high-level quantum calculation MP2, CCSD(T) and vdW-DF methods [52–54], the energies computed by the LDA functional, show some differences for the minimum values for the BZ-BZ_FF settings. These differences are due to the dispersion, and van der Waals (vdW) forces are not represented with accuracy in the LDA functional. However, the DFT-LDA for parallel and TS configuration results are in quite good agreement with high level quantum calculation proposed at work [52–54]. Even in this case, the T-shaped and the SP are the preferential configurations.

For the phenol–phenol interaction, we also considered five basic configurations: (a) the face to face with parallel OH groups (phenol–phenol_FF), (b) the face to face with antiparallel OH groups (phenol–phenol_AFF), (c) the side by side (phenol–phenol_SS), (d) the T-shaped with opposing OH groups (phenol–phenol_TS$_1$), and (e) the T-shaped with confronting OH groups (phenol–phenol_TS$_2$). The interaction energy curves calculated between the phenol dimers are illustrated in Fig. 2, in units kJ/mol.

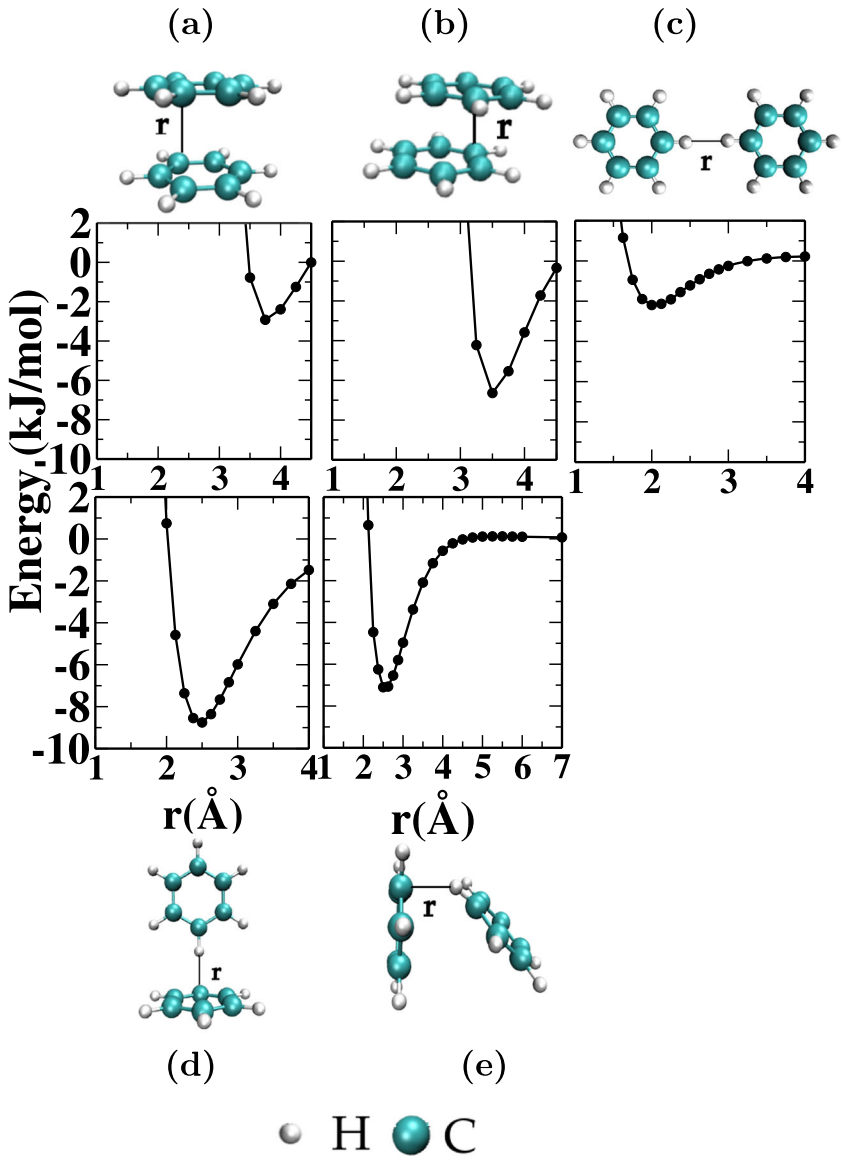

Fig. 1 Structural configurations and interaction energy curves computed for the benzene. **a** Face to face (BZ-BZ_FF). **b** Slipped parallel (BZ-BZ_SP). **c** Side by side (BZ-BZ_SS). **d** T-shaped (BZ-BZ_TS$_1$). **e** T-shaped displaced (BZ-BZ_TSD)

Between the two stacked conformations, FF and AFF, depicted in Fig. 2a and b, the second is the more stable. The phenol–phenol_AFF has its minimum energy of $-$ 5.35 kJ/mol at r = 2.75 Å, while the phenol–phenol_FF around $-$ 3.28 kJ/mol at r = 3.8 form. The energy arises from the competition between the H–π, OH–π, and π–π interactions. The difference between the two stacked configurations is due to the additional OH–OH repulsion present in the phenol-phenol_FF case. The side by side (phenol-phenol_SS) showed in the Fig. 2c is the least stable configuration since its energetics is dominated by the H–H repulsion [55–57]. The more stable structures as illustrated in the Fig. 2d and e are the phenol-phenol_TS$_1$ conformation which has its minimum at r = 2.7 Å, with energy $-$12.58 kJ/mol and the phenol-phenol_TS$_2$ with energy around $-$20.8 kJ/mol at r = 3.25 Å. These low energies arise from the H–π and OH–π electrostatic attraction.

In order to confirm that the configurations with lower energies are the T-shaped, we compared our results with the energies obtained by other functionals. Kolaski et al. [41] evaluated the interactions of the configurations the phenol–phenol employing different functionals and ab initio calculations. They obtained the binding energies between the two phenol molecules in the T-shaped configurations around $-$17.2 and $-$51 kJ/mol by optimizing the levels with MP2/CAM-B3LYP theory. According to the author, the geometry of the minimum energy is directed by the hydrogen bond formed by two hydroxyl groups and the H–π interaction between two aromatic rings as in our case. Our results for the minimum of the T-shaped configurations are

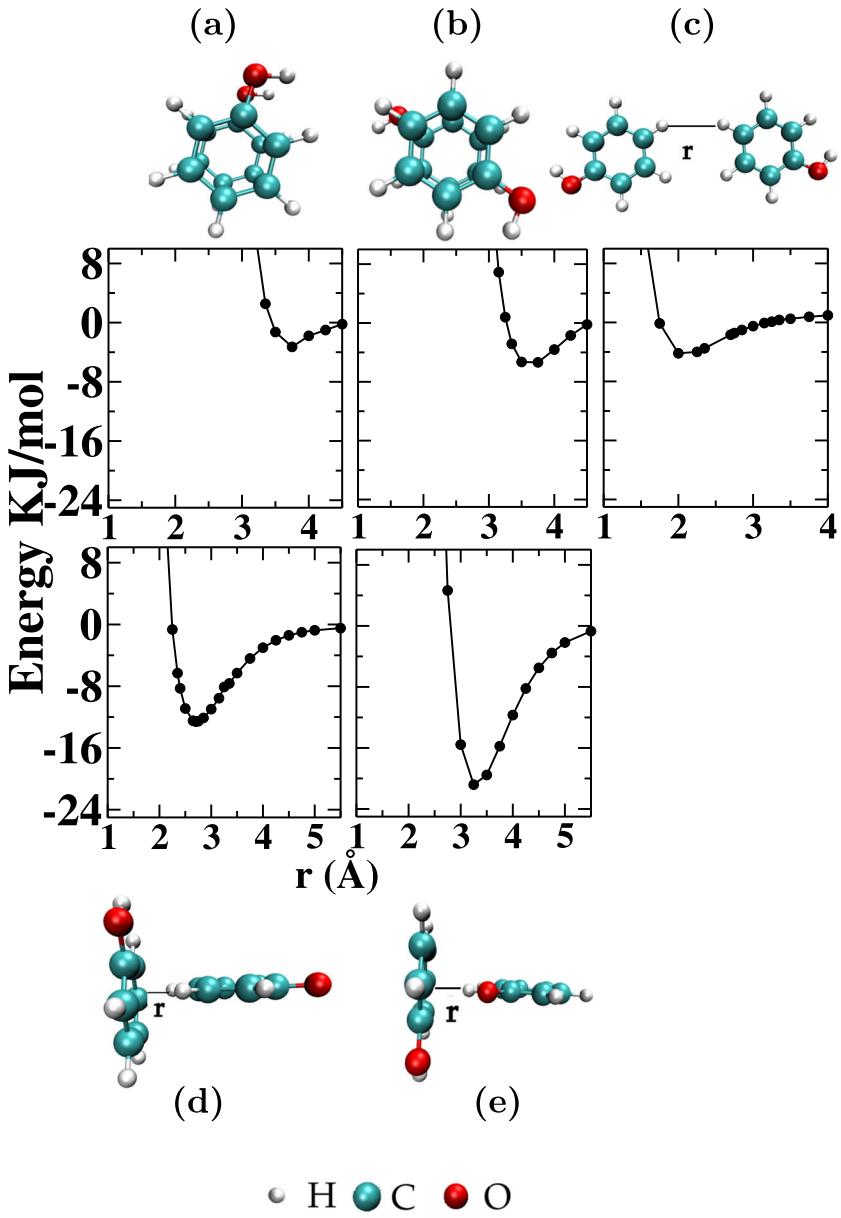

Fig. 2 Structural configurations and interaction energy curves of phenol dimer, for the five configurations. **a** Phenol–phenol_FF. **b** Phenol–phenol_AFF. **c** Phenol–phenol_SS. **d** Phenol-phenol_TS_1. **e** Phenol-phenol_TS_2

in the range of values computed by their work and provide energies for different distances as well.

In the case of the catechol–catechol interaction energy, the two OH groups expand the configurational space and we computed the energy for different distances of eight different configurations: (a) face to face (catechol-catechol_FF), (b) antiparallel face to face (catechol-catechol_AFF), (c) side by side with opposing OH groups (catechol-catechol_SS_1), (d) side by side with confronting OH groups (catechol-catechol_SS_2), (e) T-shaped with opposing OH group (catechol-catechol_TS_1), (f) T-shaped with confronting OH groups (catechol-catechol_TS_2), (g) T-shaped displaced (catechol-catechol_TSD), and (h) T-shaped with OH groups displaced (catechol-catechol_TS_3).

The comparison between the interaction energies curves of the eight configurations the catechol dimers is illustrated in Fig. 3. In these systems, a strong electrostatic attraction between the π cloud and the OH and H is present. The configuration which combines a small distance between the OH–π is the T-shaped. Within the three TS cases, the most stable configuration is the catechol-catechol_TS_3 with an energy minimum of -31.2 kJ/mol at $r = 2.25$ Å. This value is smaller than the similar catechol-catechol_TS_2, with energy value of -15.8 kJ/mol at $r = 2.5$ Å. A comparable behavior was observed in the work of Barone et al. [58].

Among the two parallel configurations catechol-catechol_FF and catechol-catechol_AFF, the second is more stable with interaction energy value of -7.41 kJ/mol

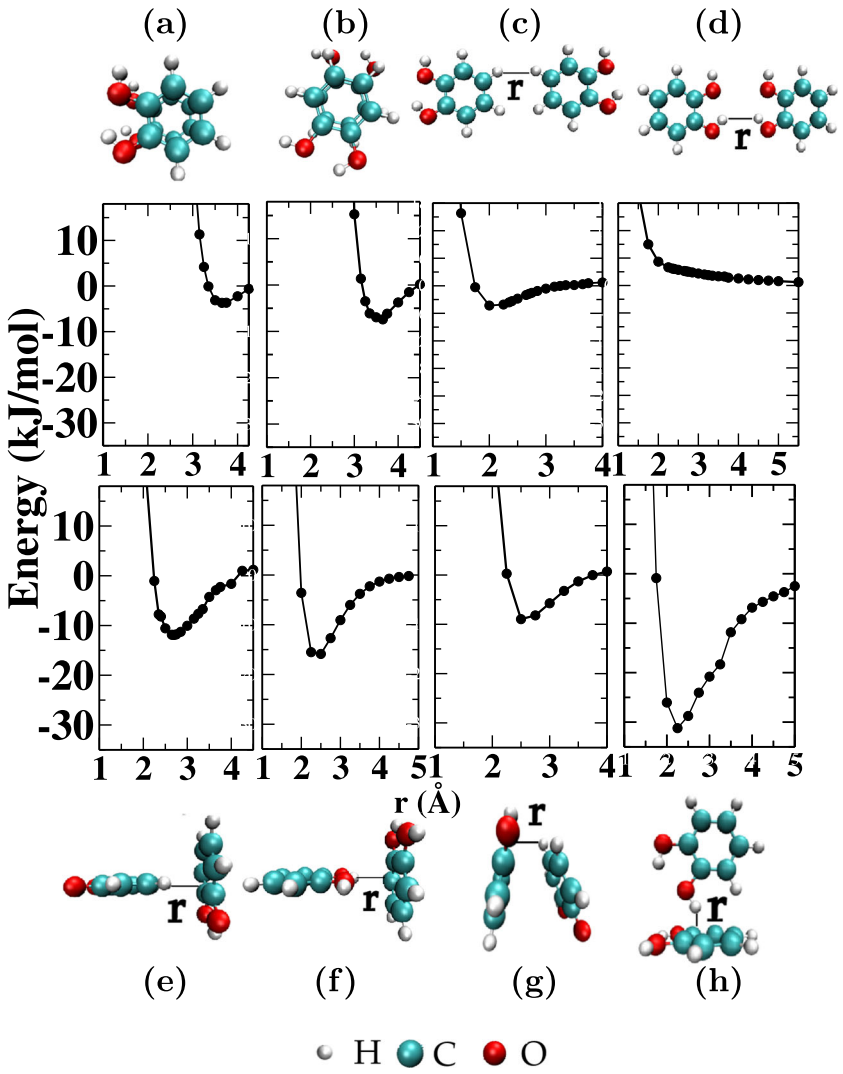

Fig. 3 Structural configurations and interaction energy curves of catechol dimer, for eight configuration. **a** Face to face . **b** Antiparallel face to face (catechol-catechol_AFF). Side by side (SS) dimers **c** catechol-catechol_SS_1 and **d** catechol-catechol_SS_2. T-shaped (TS) dimers **e** catechol-catechol_TS_1, **f** catechol-catechol_TS_2, and **g** catechol-catechol_TSD. **h** Catechol-catechol_TS_3

at $r = 3.65$ Å, in agreement with the repulsive interaction between the OH dipoles, present in the catechol-catechol_FF value of −3.69 kJ/mol at $r = 3.65$ Å form; the same behavior is observed in the study [58]. The system side by side, the catechol-catechol_SS_1, is more stable with interaction energy of −4.31 kJ/mol at $r = 2$ Å, in agreement with the strong repulsive interaction between the four OH dipoles in the catechol-catechol_SS_2 configuration. The catechol-catechol_FF has larger interaction energy than the benzene-benzene_FF and phenol-phenol_FF dimer. The two hydroxyl groups are electron-donating substituent, leading to the decrease of electrostatic repulsion between aromatic rings. The substituent effects are additive for these FF homodimers.

In a recent study, Barone et al. [58] investigated the energy of interaction between the catechol dimers using $MP2_{mod}$ and CCSD(T)/CBS methods, through four distinct configurations, similar to the investigated in our work. In the catechol-catechol_FF, catechol-catechol_AFF, catechol-catechol_TS_2, and catechol-catechol_TS_3 configurations, the energies for configurations correspond −9.62, −15.9, −17, and −21 kJ/mol, respectively. The binding energy values found in our study are below the values found in the study proposed by Barone et al. [58]. This difference is attributed to the methodology, exchange-correlation functional, and the basis sets used in each work. The neglecting flexibility of dimers catechol does not allow the OH group which can rotate and displace the H atom out of the aromatic plane to form a hydrogen bond with the other monomer, hence stabilizing the complex. As a matter of fact, Barone et al. [58] work shows the importance of such mechanism in the stability of catechol dimers. However, this is not a problem for the parameterization of force fields suitable for classical simulations.

For the calculation of the dopamine–dopamine (DA-DA) interaction energy, we selected six different configurations:

(a) face to face with parallel rings (DA-DA_FF$_1$), (b) face to face with dislocated rings (DA-DA_FF$_2$), (c) side by side (DA-DA_SS), (d) T-shaped (TS) with opposing hydroxyls (DA-DA_TS$_1$), (e) T-shaped with two NH_2 groups pointing towards the other ring (DA-DA_TS$_2$), and (f) T-shaped with one NH_2 group pointing towards the other ring (DA-DA_TS$_3$). The interaction energy curves calculated between the dopamine dimers are illustrated in Fig. 4, in units kJ/mol. The most attractive configurations are T-shaped DA-DA_TS$_2$ (energy of −24.76 kJ/mol at r = 2.7 Å), DA-DA_TS$_3$ (energy −14.75 kJ/mol at r = 2.7 Å), DA-DA_TS$_1$ (energy of −10.28 kJ/mol at r = 2.5 Å), respectively. The stability of the configurations is dominated by the NH_2 interaction with the aromatic ring, which differs from the benzene–benzene, phenol–phenol, and cathecol–cathecol interactions dominated by the OH–π and H–π interactions. This behavior is due to the influences of the amine groups and the by ethyl interactions, which is not in the same plane as the catechol of the molecule, similar to the study of L-tyrosine dimers [59].

Table 1 shows the values of the interaction energy between the homodimers for the FF, SP, and TS configurations. Even though the benzene, phenol, catechol, and dopamine exhibit different electronic structures, our study suggest that these systems share similar configurations of minimum energy T-shaped and parallel dimers. The relevant interactions in all cases are the negatively charged π-electron cloud above the ring center, where the FF (TS) configuration interaction of the electronic cloud is parallel (90°) increasing (decreasing) repulsion between the dimers. Electron-withdrawing substituents should reduce the negative π charge and lead to decreased $\pi - \pi$ electrostatic repulsion, and vice versa for electron-donating substituents [55–57, 60]. Indeed, this occurs for phenol–phenol, catechol–catechol, and dopamine–dopamine interactions. The hydroxyl group is electron-donating sub-

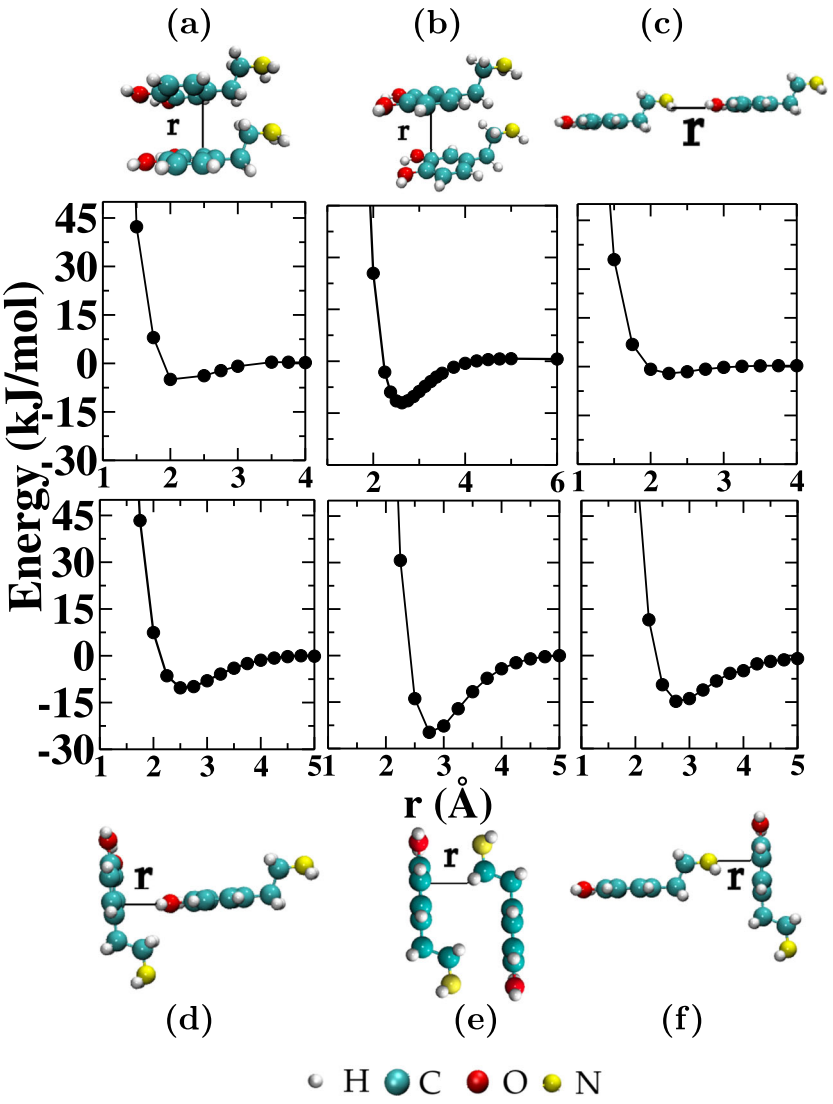

Fig. 4 Structural configurations and interaction energy curves computed for the dopamine dimer in **a** DA-DA_FF$_1$ and **b** DA-DA_FF$_2$; **c** Side by side (DA-DA_SS); and T-shaped (DA-DA_TS) dimers **d** DA-DA_TS$_1$, **e** DA-DA_TS$_2$, and **f** DA-DA_TS$_3$ configurations

Table 1 Configurations, interaction energies, and distances for benzene, phenol, catechol, and dopamine homodimers

Configurations	Energy (kJ/mol)	Distance (Å)
Face to face		
Benzene	−2.97	3.75
Phenol	−3.28	3.8
Catechol	−3.69	3.65
Dopamine	−4.2	2.0
Slipped parallel		
Benzene	−6.63	3.5
Phenol	−5.35	2.75
Catechol	−7.41	3.65
Dopamine	−6.25	2.5
T-shaped		
Benzene_TS_1	−9.0	2.5
Benzene_TSD	−7.2	2.5
Phenol_TS_1	−12.58	2.7
Phenol_TS_2	−20.8	3.25
Catechol_TS_1	−12.65	2.75
Catechol_TS_3	−21.0	2.25
Dopamine_TS_3	−14.75	2.7
Dopamine_TS_2	−24.76	2.7

stituent, leading to the decrease of electrostatic repulsion between molecule and molecule. The substituents in benzene ring have an additive effect (decreasing repulsion) on the interacting energy of face to face dimers, in the case catechol-catechol_FF when substituents are two hydroxyls. This behavior is attributed to repulsion between the dipoles of four OH group. The energetics of substituted TS configurations are more stable than benzene-benzene_TS. Among all TS configurations studied, the catechol-catechol_TS_3 arrangement is more stable than other molecule–molecule configurations, due to the contribution of the π–π and OH–π in this arrangement.

The benzene–benzene, phenol–phenol, catechol–catechol, and dopamine–dopamine dimers are ideal candidates to test the capability of new computational approaches to accurately represent the different kinds of interactions of dimers, occurring in the presence of π–π and X–π, and charge transfer interactions between these species are also an important role in the parameterization of force fields derived from calculations suitable for classical simulations [23, 26, 49, 61]. In this case, it is very important that each system has several configurations and that for a long distance (at a range $4-6$ Å) the quantum interaction energy tends to zero. The dimers studied have some important characteristics for modeling process: they are small, have OH and NH_2 groups, and dissociate in water [62, 63]. The presence of these two groups produces an electrostatic interaction and hydrogen bonds with water and graphene. Our results are therefore expected to support the crystal engineering, supramolecular chemistry, bioinspired materials, and parameterization of force fields derived from calculations suitable for classical simulations.

Molecule-graphene interaction

First, we examine the energy interaction between graphene and benzene. Among many possible configurations, we concentrate on three: two face to face (BZ-BZ_FF_1 and BZ-BZ_FF_2) and one perpendicular (BZ-BZ_CR). The interaction energy curves calculated between the benzene and the graphene are illustrated in Fig. 5, in units kJ/mol. In the BZ-BZ_FF_1 stacking case, illustrated in the Fig. 5a, the aromatic ring of the adsorbate faces the graphene hexagons, and the hydrogen atom binding to the benzene group is on top of a graphene carbon atom. In the BZ-BZ_FF_2 stacking configuration, showed in the Fig. 5b, the center of the aromatic ring of the molecule is on top of a graphene carbon atom which is similar to the configuration studies by Chakarova et al. [64]. Both BZ-GR_FF_1 and BZ-GR_FF_2 stacking configurations have very similar electronic structures with minima energies at −22 kJ/mol and −27 kJ/mol and at the equilibrium separation r = 3.5 Å, respectively. The BZ-GR_FF_1 configuration optimizes the $\pi - \pi$ stacking. The adsorption energy of BZ-GR_FF_2 in graphene was confirmed to be more stable by Tournus et al. [24], which obtained −22.9 kJ/mol obtained using the LDA of the DFT/BSSE with the SIESTA code and by Alzahrani [65] which computed −28.95 kJ/mol using the LDA of the DFT with a plane wave basis set as implemented in the Quantum ESPRESSO [66]. In the BZ-BZ_CR arrangement, depicted in Fig. 5c, the benzene is perpendicular to the graphene sheet. This configuration has a binding energy of −13 kJ/mol at r = 2.5 Å which is larger than the energy of the face to face case. The $\pi - \pi$ stacking, in this particular arrangement, is more attractive than the H–π cloud case probably due to the lower number of π bonds in the graphene when compared with the benzene. This generates a smaller charge distribution in the center of the ring that makes the interaction with H less attractive [24, 50, 65, 67].

Then, we evaluated the energy between a phenol and graphene sheet. The following configurations were

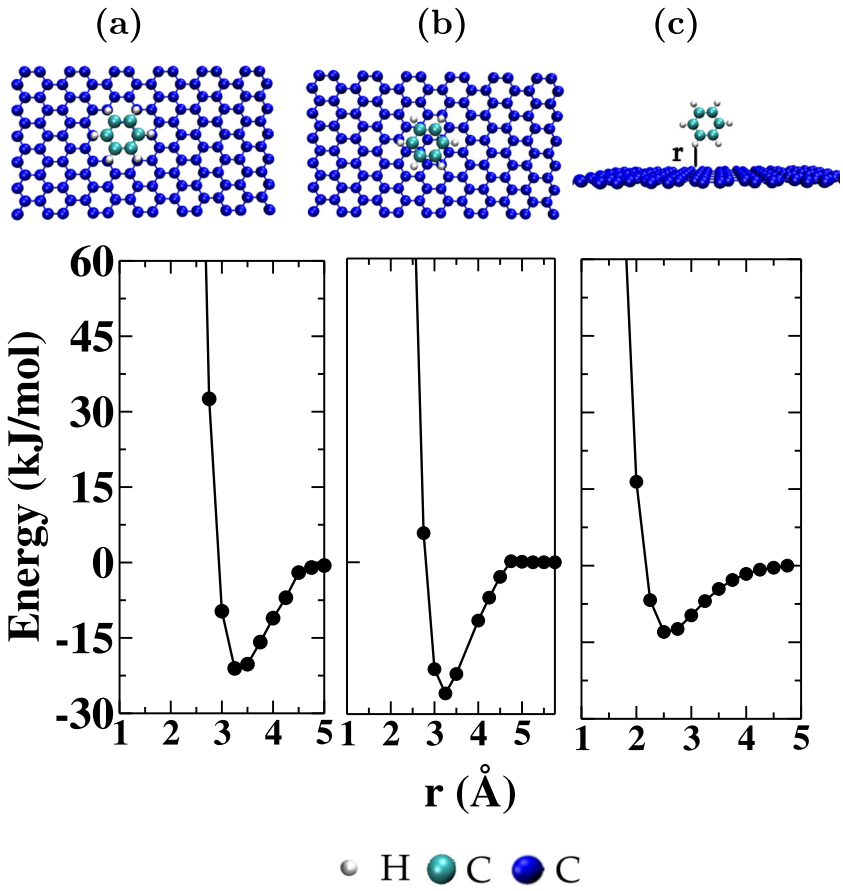

Fig. 5 Structural configurations and interaction energy curves for the benzene molecule above the graphene layer. **a** BZ-GR_FF$_1$. **b** BZ-GR_FF$_2$. **c** BZ-GR_CR. The distance (r) is measured from the benzene molecule to the graphene layer

considered: one face to face (phenol-GR_FF) and two perpendicular configurations (phenol-GR_CR$_1$ and phenol-GR_CR$_2$). The interaction energy curves calculated between the phenol and the graphene are illustrated in Fig. 6, in units kJ/mol. In the phenol-GR_FF case, the aromatic ring of the phenol faces the graphene hexagons directly as showed in the Fig. 6a. In one of the perpendicular orientations, the phenol-GR_CR$_1$, the group OH of the phenol points to the graphene ring as shown in Fig. 6b while in the other perpendicular orientation phenol-GR_CR$_2$, the H group points to the graphene ring, as indicated in the Fig. 6c.

The minimum of the phenol–graphene interaction in the face to face configuration is −24 kJ/mol at r=3.25 Å, while for the phenol-GR_CR$_1$ and phenol-GR_CR$_2$ correspond to −18.43 kJ/mol (2.25 Å) and −12 kJ/mol (2.75 Å), respectively. Comparing all the configurations analyzed, the lowest energy is the face to face due to the π-π stacking. Within the two perpendicular configurations, the phenol-GR_CR$_1$ exhibits the lower minimum since the electrostatic attraction between the OH and the negative cloud in the center of the graphene ring is stronger than the attraction between the H and the π cloud.

Computational simulation by Hernandez et al. [68] reveals that the pristine phenol-graphene interaction has a minimum of −8.104 kJ/mol. The author evaluated six different configurations, using a different methodology compared with this work, analyzed through the Quantum ESPRESSO package [66] and used GGA [47], which tends to underestimate the binding energy values [69]. As the most stable configuration was obtained with phenol parallel to graphene (π–π type interaction) at a distance of r = 4.07 Å. Using similar methodology, Avila et al. [70] who evaluated the interaction of phenol with pristine graphene in three configurations observed that the most stable one is FF similar to that we evaluated phenol-graphene_FF, the adsorption energy values of −4.650 kJ/mol and vdW-DF adsorption energy of about −75.14 kJ/mol; however, no BSSE was performed.

Next, we calculated the catechol–graphene energy as a function of the distance between them. We studied four configurations: one face to face (catechol-GR_FF) and three

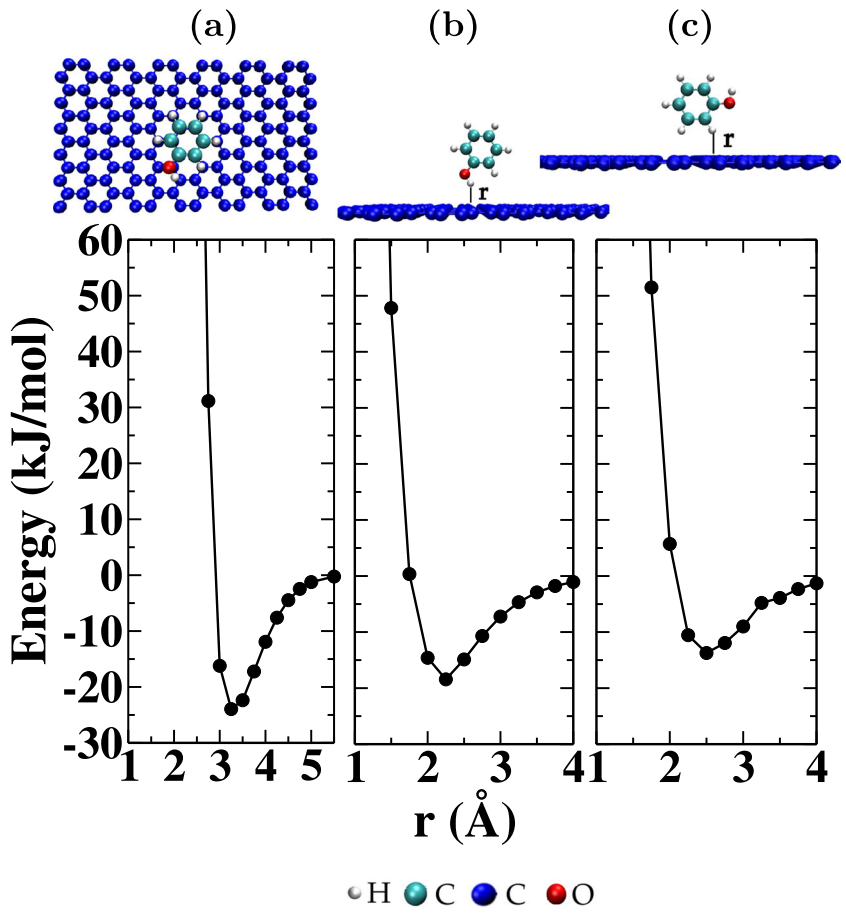

Fig. 6 Structural configurations and interaction energy curves for the phenol molecule above the graphene layer. **a** phenol-GR_FF. **b** phenol-GR_CR$_1$. **c** Phenol-GR_CR$_2$. The distance (r) is measured from the phenol molecule to the graphene layer

perpendicular configurations (catechol-GR_CR$_1$, catechol-GR_CR$_2$, and catechol-GR_CR$_3$). Figure 7 shows the calculated interaction energies as a function of the distance in units kJ/mol. For the minimum energy for the catechol-GR_FF, illustrated in Fig. 7a, we found −26.7 kJ/mol at the equilibrium separation r = 3.25 Å. As in the previous cases, this behavior is attributed to the attractive interaction $\pi - \pi$. The perpendicular orientations, catechol-GR_CR$_1$, catechol-GR_CR$_2$, and catechol-GR_CR$_3$ shown in Fig. 7b, c, and d present energies of −20.25, −13.75, and −16 kJ/mol at 2.25, 2.5, and 2.75 Å, respectively. The catechol-GR_CR$_1$ is the most attractive configuration between the perpendicular orientations. The H and the OH are electrostatically attracted to the electronic charges at the center of the graphene ring. However, since the hydrogen in the OH linked to the C is more polarized than the H covalent linked to the C, the configuration in which the OH points towards the center of the graphene ring is the lower in energy.

Our results can be qualitatively compared with other methods. The case of the binding energy of a catechol interaction energy was approximate molecule absorbed on a silica surface analyzed using DFT/BSSE functionals with the SIESTA code [71, 72], show that the catechol in the face to face configuration adhered stronger to the silica surface than other configurations with energy of −96.2 kJ/mol. They also observed the presence of catechol adhesion arising from both the OH groups interacting with the aromatic ring and the $\pi - \pi$ stacking [72].

Finally, we evaluated the graphene dopamine interaction in four different configurations: two face to face (DA-GR_FF$_1$ and DA-GR_FF$_2$) and two perpendicular (DA-GR_CR$_1$ and DA-GR_CR$_2$). Figure 8 shows the calculated interaction energies as a function of the distance in units kJ/mol. The most stable system was the DA-GR_FF$_1$ (approaching the $-NH_2$ group and the parallel aromatic ring) in the distance of 2.75 Å and the interaction energy was approximately −35 kJ/mol. In this configuration, the

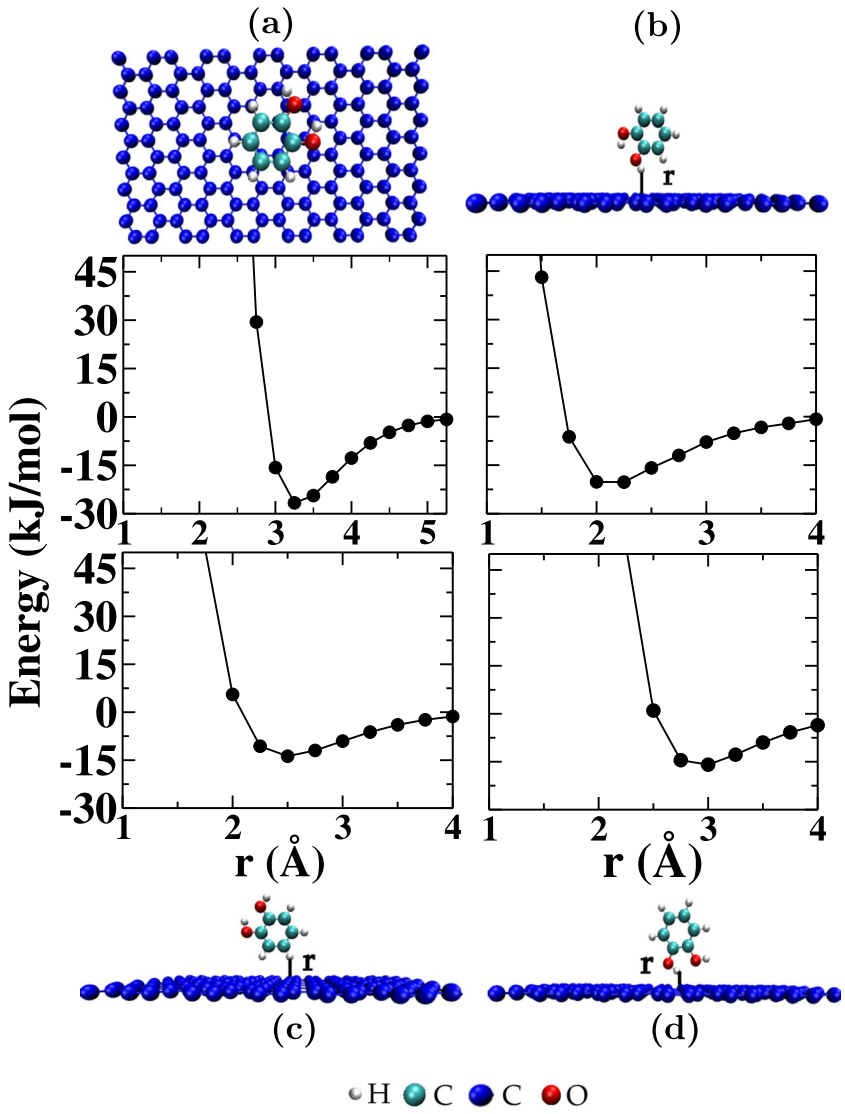

Fig. 7 Structural configurations and interaction energy curves for a catechol molecule on graphene sheet. **a** Catechol-GR_FF. **b** Catechol-GR_CR$_1$. **c** Catechol-GR_CR$_2$. **d** Catechol-GR_CR$_3$. The distance (r) is measured from the catechol molecule to the graphene layer

aromatic ring of dopamine is dislocated with reference to the graphene allowing both a $\pi - \pi$ and a $-NH_2$–π-cloud interaction. The minimum of the DA-GR_FF$_2$ configuration is −31.3 kJ/mol at r = 3.25 Å. In the perpendicular configurations, the DA-GR_CR$_1$ shows minimum energy is around −30 kJ/mol at 3.25 Å.

Using similar methodology Rossi et al. [73] evaluated the interaction of dopamine with pristine graphene in six configurations, observed that in the aromatic ring can be the most stable was two face to face arrangements. The face to face configurations similar to that we evaluated DA-GR_FF$_2$, the DFT-D2 adsorption energy of about −67.54 kJ/mol; however, no BSSE was performed. The distance between the dopamine ring and graphene was almost 3.18–3.30 Å. Furthermore, in a DFT/6-31G** studies [74] on an DA-GR_FF$_1$ system performed without BSSE, the calculated adsorption energy was approximately −145.69 kJ/mol and distance between DA-GR was about 3.4 Å. Other studies [75] with aromatic molecules as in the case of nucleobases in graphene show that the distance with greater stability between the aromatic ring and the graphene is around 3.2 Å.

Li et al. [76] investigated the adsorption of aromatic molecules on graphene. They observed, via MD simulations, that the effect of substituent groups on the aromatic ring increases the adsorption on graphene and have the

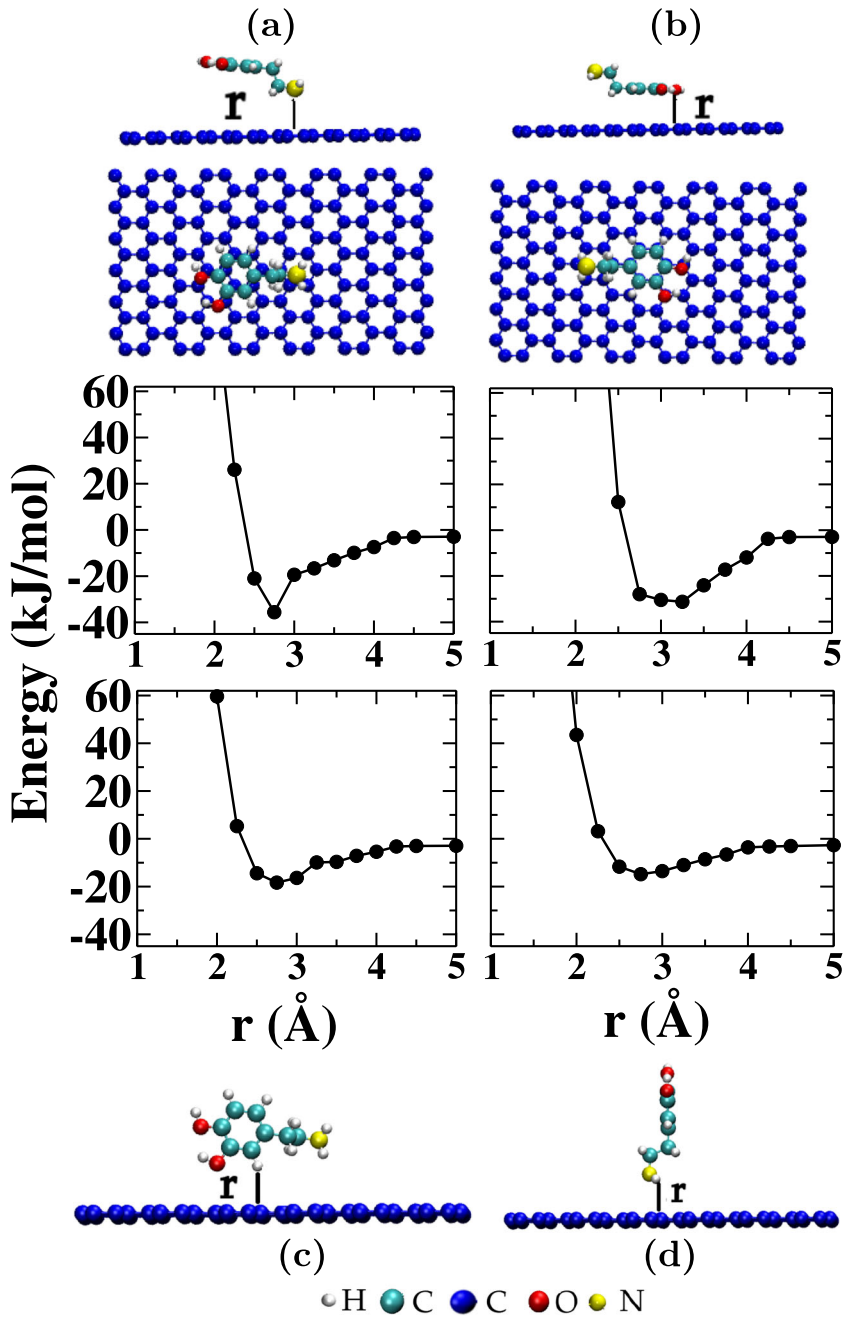

Fig. 8 Structural configurations and interaction energy curves for the dopamine molecule above the graphene layer. **a** DA-Gr_FF$_1$. **b** DA-Gr_FF$_2$. **c** DA-Gr_CR$_1$. **d** DA-Gr_CR$_2$. The distance (r) is measured from the dopamine to the graphene layer

following order: nitrobenzene (−27.8 kJ/mol) > anisole (−23.7 kJ/mol) > chlorobenzene (−22.9 kJ/mol) > phenol (−22.1 kJ/mol) > aniline (−17.6 kJ/mol) > benzene (−16.7 kJ/mol). In addition, the authors show through the rupture forces of molecule–graphene that there may be a strong resonance effect between the aromatic ring and the hydroxyl group.

Table 2 shows the values of the adsorption energy of a molecule on graphene. The adsorption energy has the following order: dopamine > catechol > phenol > benzene. The hydroxyl group has a strong effect for aromatic ring adsorption on graphene [76]. The FF configurations are the stable for molecule–graphene systems, due to the favoring of π–π interactions in these arrangements. The dopamine binding energy to graphene (FF and CR arrangements) is more stable than other molecules, due to the contribution of the $\pi - \pi$, OH-π, and $-NH_2$ interactions.

Our results suggest that in the interaction between the graphene and the molecules, the face to face arrangements are the most stable structures. The dopamine binds to

Table 2 Configurations, interaction energies, and distances for benzene-GR, phenol-GR, catechol-GR, and dopamine-GR

Configurations	Energy (kJ/mol)	Distance (Å)
FF		
Benzene-GR	−22.0	3.5
Phenol-GR	−24.0	3.25
Catechol-GR	−26.7	3.25
Dopamine-GR_FF$_1$	−35.0	2.75
CR		
Benzene-GR	−13.0	2.5
Phenol-GR_CR$_1$	−18.43	2.25
Catechol-GR_CR$_1$	−20.25	2.25
Dopamine-GR_CR$_1$	−30.0	3.25

graphene more stable when compared with other molecules, due to the contribution of the $\pi - \pi$, OH-π, and –NH_2 interactions. This indicates that this molecule would be interesting for drug delivery and filters based in graphene.

Conclusions

We applied DFT with the LDA functional to evaluate the interaction energies between benzene–benzene, phenol–phenol, catechol–catechol, dopamine–dopamine, benzene–graphene, phenol–graphene, catechol–graphene, and dopamine–graphene systems. The interaction energy between dimers is determined mainly by the directionality of $\pi - \pi$ and X–π interactions in these systems.

The T-shaped configurations are the most stable among the molecule–molecule interaction configurations, due to the fact of favoring the multipoles in this arrangement, decreasing repulsion between π-electron from the electronic cloud of the dimers. The energetics of substituted T-shaped configurations are more stable than benzene-benzene_TS$_1$. Among all T-shaped configurations studied, the catechol-catechol_TS$_3$ arrangement is more stable than other molecule–molecule configurations, due to the contribution of the π–π and OH–π in this arrangement. The substituent effects of –OH, two OH, or –NH_2 groups on the aromatic ring in face to face arrangement decrease the repulsion between molecule–molecule interacting. These results provide insight into the manner by which substituents X–π in the aromatic ring can be utilized in the supramolecular design.

The adsorption energy of a molecule on graphene involves weak $\pi - \pi$ interactions. The face to face configurations are the most stable for molecule–graphene systems, due to the favoring of π–π interactions in these arrangements. The substituent groups effect can strengthen the FF interaction when compared with the unsubstituted benzene dimer. The dopamine binding energy to graphene is more stable than other molecules, due to the contribution of the $\pi - \pi$, OH–π, and –NH_2 interactions. The molecule-graphene_FF distance around 3.2 Å is of the same order as the usual separation between two sp^2 systems, interplanar distance in graphite.

Consequently, in a three-body configuration, the lowest energy is not the additive combination of the lowest energy of the molecule–molecule and the molecule–graphene interaction, but is a combination of all the presented configurations in some balance. Therefore, in the modeling of a proper carrier, all the presented configurations have to be taken into account with an appropriated thermal balance. This analysis is relevant for parameterization of force fields derived from calculations suitable for classical simulations.

Our results are therefore expected to support the design of novel sensing, drug delivery, and filters based in graphene. The substituent effects of aromatic ring provide insight into the manner by which substituents X–π on the aromatic ring can be utilized in the supramolecular design and crystal engineering, bioinspired materials, formation of various molecular agglomerates, and parameterization of force fields suitable for classical simulations.

References

1. Iijima S, Ichihashi T (1993) Single-shell carbon nanotubes of 1-nm diameter. Nature 363:603
2. Moraes EE, Manhabosco TM, De Oliveira AB, Batista RJ (2012) Tunable band gap of boron nitride interfaces under uniaxial pressure. J Phys: Condens Matter 24:475502
3. Moraes EE, Coutinho-Filho MD, Batista RJ (2017) Transport properties of hydrogenated cubic boron nitride nanofilms with gold electrodes from density functional theory. ACS Omega 2(4):1696–1701
4. Novoselov KS, Geim AK, Morozov SV, Jiang D, Zhang Y, Dubonos SV, Grigorieva IV, Firsov AA (2004) Electric field effect in atomically thin carbon films. Science 306:666–669
5. Neto AC, Guinea F, Peres NM, Novoselov KS, Geim AK (2009) The electronic properties of graphene. Rev Mod Phys 81:109
6. Rao C, Sood A, Subrahmanyam K, Govindaraj A (2009) Graphene: the new two-dimensional nanomaterial. Angew Chem Int Ed 48:7752–7777
7. Gan T, Hu S (2011) Electrochemical sensors based on graphene materials. Microchim Acta 175:1
8. Tonel M, Lara I, Zanella I, Fagan S (2017) The influence of the concentration and adsorption sites of different chemical groups on graphene through first principles simulations. Phys Chem Chem Phys 19:27374–27383
9. Tonel MZ, Martins MO, Zanella I, Pontes RB, Fagan SB (2017) A first-principles study of the interaction of doxorubicin with graphene. Comput Theor Chem 1115:270–275
10. Chen RJ, Bangsaruntip S, Drouvalakis KA, Kam NWS, Shim M, Li Y, Kim W, Utz PJ, Dai H (2003) Noncovalent functionalization of carbon nanotubes for highly specific electronic biosensors. Proc Natl Acad Sci 100:4984–4989

11. Kang HS (2005) Theoretical study of binding of metal-doped graphene sheet and carbon nanotubes with dioxin. J Am Chem Soc 127:9839–9843
12. Gowtham S, Scheicher RH, Ahuja R, Pandey R, Karna SP (2007) Physisorption of nucleobases on graphene: density-functional calculations. Phys Rev B 76:033401
13. Varghese N, Mogera U, Govindaraj A, Das A, Maiti PK, Sood AK, Rao C (2009) Binding of dna nucleobases and nucleosides with graphene. Chem Phys Chem 10:206–210
14. Cazorla C (2010) Ab initio study of the binding of collagen amino acids to graphene and a-doped (a= h, ca) graphene. Thin Solid Films 518:6951–6961
15. Umadevi D, Sastry GN (2011) Quantum mechanical study of physisorption of nucleobases on carbon materials: graphene versus carbon nanotubes. J Phys Chem Lett 2:1572–1576
16. Cazorla C, Rojas-Cervellera V, Rovira C (2012) Calcium-based functionalization of carbon nanostructures for peptide immobilization in aqueous media. J Mat Chem 22:19684–19693
17. Vovusha H, Sanyal S, Sanyal B (2013) Interaction of nucleobases and aromatic amino acids with graphene oxide and graphene flakes. J Phys Chem Lett 4:3710–3718
18. Chen L, Li X, Tanner EE, Compton RG (2017) Catechol adsorption on graphene nanoplatelets: isotherm, flat to vertical phase transition and desorption kinetics. Chem Sci 8:4771–4778
19. Li D, Müller MB, Gilje S, Kaner RB, Wallace GG (2008) Processable aqueous dispersions of graphene nanosheets. Nat Nanotechnol 3:101
20. Dong X, Fu D, Fang W, Shi Y, Chen P, Li L-J (2009) Doping single-layer graphene with aromatic molecules. Small 5:1422–1426
21. Wu T, Cai X, Tan S, Li H, Liu J, Yang W (2011) Adsorption characteristics of acrylonitrile, p-toluenesulfonic acid, 1-naphthalenesulfonic acid and methyl blue on graphene in aqueous solutions. Chem Eng J 173:144–149
22. Hwang YH, Chun HS, Ok KM, Lee K-K, Kwak K (2015) Density functional investigation of graphene doped with amine-based organic molecules. J Nanomater 2015:5
23. Kong L, Román-Pérez G, Soler JM, Langreth DC (2009) Energetics and dynamics of h 2 adsorbed in a nanoporous material at low temperature. Phys Rev Lett 103:096103
24. Cacelli I, Cinacchi G, Prampolini G, Tani A (2004) Computer simulation of solid and liquid benzene with an atomistic interaction potential derived from ab initio calculations. J Am Chem Soc 126:14278–14286
25. Amovilli C, Cacelli I, Cinacchi G, De Gaetani L, Prampolini G, Tani A (2007) Structure and dynamics of mesogens using intermolecular potentials derived from ab initio calculations. Theor Chem Acc 117:885–901
26. Cacelli I, Cimoli A, Livotto PR, Prampolini G (2012) An automated approach for the parameterization of accurate intermolecular force-fields: pyridine as a case study. J Comput Chem 33:1055–1067
27. Hobza P, Selzle HL, Schlag EW (1994) Structure and properties of benzene-containing molecular clusters: nonempirical ab initio calculations and experiments. Chem Rev 94:1767–1785
28. Bieske EJ, Dopfer O (2000) High-resolution spectroscopy of cluster ions. Chem Rev 100:3963–3998
29. Tarakeshwar P, Kim KS, Brutschy B (2001) σ to π conformational transition: interactions of the water trimer with π systems. J Chem Phys 114:1295–1305
30. Guin M, Patwari GN, Karthikeyan S, Kim KS (2009) A π-stacked phenylacetylene and 1, 3, 5-triazine heterodimer: a combined spectroscopic and ab initio investigation. Phys Chem Chem Phys 11:11207–11212
31. Hoeben FJ, Jonkheijm P, Meijer E, Schenning AP (2005) About supramolecular assemblies of π-conjugated systems. Chem Rev 105:1491–1546
32. Cerný J, Kabelác M, Hobza P (2008) Double-helical ladder structural transition in the b-dna is induced by a loss of dispersion energy. J Am Chem Soc 130:16055–16059
33. Meyer EA, Castellano RK, Diederich F (2003) Interactions with aromatic rings in chemical and biological recognition. Angew Chem Int Ed 42:1210–1250
34. Lee JY, Hong BH, Kim WY, Min SK, Kim Y, Jouravlev MV, Bose R, Kim KS, Hwang I-C, Kaufman LJ et al (2009) Near-field focusing and magnification through self-assembled nanoscale spherical lenses. Nature 460:498
35. Vaupel S, Brutschy B, Tarakeshwar P, Kim KS (2006) Characterization of weak nh- π intermolecular interactions of ammonia with various substituted π-systems. J Am Chem Soc 128:5416–5426
36. Tarakeshwar P, Choi HS, Kim KS (2001) Olefinic vs aromatic π-h interaction: a theoretical investigation of the nature of interaction of first-row hydrides with ethene and benzene. J Am Chem Soc 123:3323–3331
37. Hohenstein EG, Sherrill CD (2009) Effects of heteroatoms on aromatic π- π interactions: benzene- pyridine and pyridine dimer. J Phys Chem A 113:878–886
38. Piacenza M, Grimme S (2005) Van der waals complexes of polar aromatic molecules: unexpected structures for dimers of azulene. J Am Chem Soc 127:14841–14848
39. Ringer AL, Sherrill CD (2009) Substituent effects in sandwich configurations of multiply substituted benzene dimers are not solely governed by electrostatic control. J Am Chem Soc 131:4574–4575
40. Geronimo I, Singh NJ, Kim KS (2011) Can electron-rich π systems bind anions. J Chem Theory Comput 7:825–829
41. Kołaski M, Kumar A, Singh NJ, Kim KS (2011) Differences in structure, energy, and spectrum between neutral, protonated, and deprotonated phenol dimers: comparison of various density functionals with ab initio theory. Phys Chem Chem Phys 13:991–1001
42. Hohenberg P (1964) Inhomogeneous electron gas. Phys Rev B 136:864
43. Kohn W (1965) Self-consistent equations including exchange and correlation effects. Phys Rev A 140:1133
44. Soler JM, Artacho E, Gale JD, García A, Junquera J, Ordejón P, Sánchez-Portal D (2002) The siesta method for ab initio order-n materials simulation. J Phys: Condens Matter 14:2745
45. Perdew JP, Zunger A (1981) Self-interaction correction to density-functional approximations for many-electron systems. Phys Rev B 23:5048
46. Boys SF, Bernardi Fd (1970) The calculation of small molecular interactions by the differences of separate total energies. some procedures with reduced errors. Molec Phys 19:553–566
47. Perdew JP, Burke K, Ernzerhof M (1996) Generalized gradient approximation made simple. Phys Rev Lett 77:3865
48. Artacho E, Anglada E, Diéguez O, Gale JD, García A, Junquera J, Martin RM, Ordejón P, Pruneda JM, Sánchez-Portal D et al (2008) The siesta method; developments and applicability. J Phys: Condens Matter 20:064208
49. Grimme S (2006) Semiempirical gga-type density functional constructed with a long-range dispersion correction. J Comput Chem 27:1787–1799
50. Prampolini G, Livotto PR, Cacelli I (2015) Accuracy of quantum mechanically derived force-fields parameterized from dispersion-corrected dft data: the benzene dimer as a prototype for aromatic interactions. J Chem Theory Comput 11:5182–5196
51. Tournus F, Charlier J-C (2005) Ab initio study of benzene adsorption on carbon nanotubes. Phys Rev B 71:165421

52. Sato T, Tsuneda T, Hirao K (2005) A density-functional study on π-aromatic interaction: benzene dimer and naphthalene dimer. J Chem Phys 123:104307
53. Chakarova-Käck SD, Schröder E, Lundqvist BI, Langreth DC (2006) Application of van der waals density functional to an extended system: Adsorption of benzene and naphthalene on graphite. Phys Rev Lett 96:146107
54. Sinnokrot MO, Sherrill CD (2003) Unexpected substituent effects in face-to-face π-stacking interactions. J Phys Chem A 107:8377–8379
55. Tsuzuki S, Honda K, Uchimaru T, Mikami M, Tanabe K (2002) Origin of attraction and directionality of the π/π interaction: model chemistry calculations of benzene dimer interaction. J Am Chem Soc 124:104–112
56. Grover J, Walters E, Hui E (1987) Dissociation energies of the benzene dimer and dimer cation. J Phys Chem Chem 91:3233–3237
57. Sinnokrot MO, Sherrill CD (2004) Substituent effects in π- π interactions: sandwich and t-shaped configurations. J Am Chem Soc 126:7690–7697
58. Cozzi F, Siegel J (1995) Interaction between stacked aryl groups in 1, 8-diarylnaphthalenes: dominance of polar/π over charge-transfer effects. Pure Appl Chem 67:683–689
59. Cozzi F, Ponzini F, Annunziata R, Cinquini M, Siegel JS (1995) Polar interactions between stacked π systems in fluorinated 1, 8-diarylnaphthalenes: importance of quadrupole moments in molecular recognition. Angew Chem Int Ed 34:1019–1020
60. Barone V, Cacelli I, Ferretti A, Prampolini G (2017) Noncovalent interactions in the catechol dimer. Biomim 2:18
61. Purushotham U, Sastry GN (2012) Exploration of conformations and quantum chemical investigation of l-tyrosine dimers, anions, cations and zwitterions: a dft study. Theor Chem Acc 131:1093
62. Furlan A, Almarza NG, Barbosa M (2016) Lattice model for water-solute mixtures. J Chem Phys 145:144501
63. Furlan A, Lomba E, Barbosa M (2017) Temperature of maximum density and excess properties of short-chain alcohol aqueous solutions: a simplified model simulation study. J Chem Phys 146:144503
64. AlZahrani A (2010) First-principles study on the structural and electronic properties of graphene upon benzene and naphthalene adsorption. Appl Surf Sci 257:807–810
65. Giannozzi P, Baroni S, Bonini N, Calandra M, Car R, Cavazzoni C, Ceresoli D, Chiarotti GL, Cococcioni M, Dabo I et al (2009) Quantum espresso: a modular and open-source software project for quantum simulations of materials. J Phys: Condens Matter 21:395502
66. Kong L, Enders A, Rahman TS, Dowben PA (2014) Molecular adsorption on graphene. J Phys: Condens Matter 26:443001
67. Hernández JMG, Anota EC, de la Cruz MTR, Melchor MG, Cocoletzi GH (2012) First principles studies of the graphene-phenol interactions. J Mol Mod 18:3857–3866
68. Giese TJ, York DM (2010) Density-functional expansion methods: evaluation of lda, gga, and meta-gga functionals and different integral approximations. J Chem Phys 133:244107
69. Boukhvalov D (2013) Dft modeling of the covalent functionalization of graphene: from ideal to realistic models. Rsc Adv 3:7150–7159
70. Avila Y, Cocoletzi GH, Romero MT (2014) First principles calculations of phenol adsorption on pristine and group iii (b, al, ga) doped graphene layers. J Mol Model 20:2112
71. Mian SA, Saha LC, Jang J, Wang L, Gao X, Nagase S (2010) Density functional theory study of catechol adhesion on silica surfaces. J Phys Chem C 114:20793–20800
72. Mian SA, Yang L-M, Saha LC, Ahmed E, Ajmal M, Ganz E (2014) A fundamental understanding of catechol and water adsorption on a hydrophilic silica surface: exploring the underwater adhesion mechanism of mussels on an atomic scale. Langmuir 30:6906–6914
73. Fernández ACR, Castellani NJ (2017) Noncovalent interactions between dopamine and regular and defective graphene. ChemPhysChem 18(15):2065–2080
74. Zhang H-p, Lin X-y, Lu X, Wang Z, Fang L, Tang Y (2017) Understanding the interfacial interactions between dopamine and different graphenes for biomedical materials. Mater Chem Front 1(6):1156–1164
75. Antony J, Grimme S (2008) Structures and interaction energies of stacked graphene–nucleobase complexes. Phys Chem Chem Phys 10:2722–2729
76. Li Y, Liao M, Zhou J (2018) Catechol and its derivatives adhesion on graphene: insights from molecular dynamics simulations. J Phys Chem C 122:22965–22974

Publisher's note Springer Nature remains neutral with regard to jurisdictional claims in published maps and institutional affiliations.